appreciably affect the data in the region of the second minimum.

As mentioned in the Introduction, the knockout process might be expected to compete more strongly in the $^{90}Zr(p,\alpha)$ reaction, where the target ground state contains a pair of protons outside of the core state. It is possible that a knockout (p,α) reaction would be characterized by an angular distribution that is not identical to that of a pickup (p,α) reaction. It is also conceivable that the angular distributions for the two reactions would have different energy dependence. In this case variation of the bombarding energy would result in different displacements of the two diffraction patterns. This could account for the "filling in" of the second minimum of $^{90}Zr(p,\alpha_0)$ at the 20.2-MeV bombarding energy. A detailed examination of the knockout contribution must await an adequate theoretical treatment of the reaction dynamics.

The angular distribution of the first 2+ level in ^{86}Sr excited by the $^{89}Y(p,\alpha)$ reaction is compared with the ground-state angular distribution in Fig. 10. This state is probably largely due to the coupling of two $g_{9/2}$ neutron holes. The (p,α) reaction would excite this state by the pickup of two $g_{9/2}$ neutrons coupled to spin 2+ from the ^{89}Y ground state. The spectroscopic factor for this pickup is 5 (compared with 1 for the ground-state transition). As the available subroutines require the orbital angular momentum of the neutron pair to be coupled to 0, we cannot calculate the dynamic part of this transition. However, an examination of Fig. 10 shows qualitative agreement with the expected larger spectroscopic factor for the 2+ final state.

V. SUMMARY

The comparison of the experimental data with the distorted-wave calculations provides good evidence that pickup of a quasi-triton is the dominant mechanism for the (p,α) reactions to low-lying final states. This evidence is provided by the agreement of the general shapes of the experimental and calculated angular distributions, by the relative intensities of the (p,α_0) reactions in ^{89}Y and ^{90}Zr, and by the relative intensities of the (p,α_0) and (p,α_1) reactions in ^{90}Zr. It is not possible, however, to exclude completely some knockout contribution to the reaction in cases where the structure of the target nucleus is favorable for a knockout process.

ACKNOWLEDGMENTS

The authors are indebted to R. H. Bassel, R. M. Drisko, and G. R. Satchler for permission to use the code JULIE and for many valuable discussions during the course of this work.

PHYSICAL REVIEW VOLUME 140, NUMBER 2B 25 OCTOBER 1965

Photoproduction of π^0 from Hydrogen near the Second Pion-Nucleon Resonance*

H. De Staebler, Jr.,† E. F. Erickson, A. C. Hearn,‡ and C. Schaerf§
Institute of Theoretical Physics, Department of Physics and High Energy Physics Laboratory, Stanford University, Stanford, California

(Received 26 April 1965)

Angular distributions for π^0 photoproduction from hydrogen at energies between 660 and 800 MeV and proton center-of-mass angles from 0° to 140° have been measured and analyzed. Some variation from a pure $d_{3/2}$ state is seen in the resonance region. A possible high-momentum-transfer enhancement of the cross section is discussed.

I. INTRODUCTION

PION photoproduction from nucleons has proved a useful tool in the study of the pion-nucleon interaction because of the dominance of the strong final-state interaction between emitted pion and recoil nucleon. There has remained, however, a noticeable lack of data at high momentum transfer in the region of the second pion-nucleon resonance. In particular, our zero-angle measurement[1] provides evidence against the hypothesis that the direct photoelectric term is responsible for the difference in position of this resonance in π^0 and π^+ photoproduction.[2]

The present experiment was designed to study this region using the Stanford Mark III linear accelerator. The results of the experiment establish that the discrepancy in resonance positions is not due to the photo-

* Work supported in part by the U. S. Office of Naval Research, Contract Nonr 225 (67), and in part by the U. S. Air Force Office of Scientific Research, Contract AF 49(638)-1389. Computation was supported in part by National Science Foundation Grant NSF-GP948.

† Now at Stanford Linear Accelerator Center, Stanford, California.

‡ Now at National Aeronautics and Space Administration, Ames Research Center, Moffett Field, California.

§ Now at Laboratori Nazionali di Frascati, Frascati (Roma), Italy.

[1] Throughout this paper, the angle between incident photon and final recoil proton will be used (θ^* is the center-of-mass angle and θ the laboratory angle).

[2] A. M. Wetherall, Phys. Rev. 115, 1722 (1959).

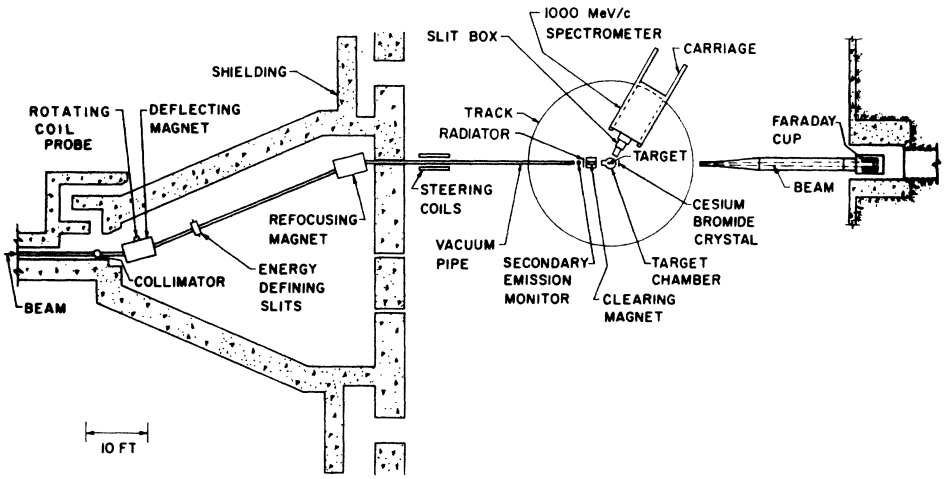

FIG. 1. Diagram of experimental layout (see text).

electric term, and also establish the possibility of a high-momentum-transfer enhancement of π^0 photoproduction caused by crossed-nucleon and nucleon-isobar exchanges.

The paper is divided into five parts. In Sec. II, the experimental equipment and techniques are described. Section III contains an account of the data reduction, and the results are then interpreted in Sec. IV. Finally, in Sec. V, general conclusions are drawn.

II. EXPERIMENTAL EQUIPMENT AND PROCEDURE

In Fig. 1. we have schematically indicated the layout of the apparatus used in this experiment. A description of the various components follows.

A. Electron Beam

Electrons from the Stanford Mark III linear accelerator were collimated by a 0.125-in.-diam hole in a 1.33-in.-thick copper or iron collimator, and then passed successively through a deflecting magnet, energy-defining slits, and bending magnet before reaching the experimental area (or "end station"). This momentum-analyzing system is described in detail in Ref. 3, and its calibration is probably better than $\pm 1\%$.[4] The energy-defining slits were set to accept a 1% interval of the incident-electron momentum spectrum at the nominal value of the transmitted momentum. The current in the deflecting magnet was set with a potentiometer which read the voltage on a shunt in series with the magnet windings, the field in the deflecting magnet being monitored by a proton-resonance regulated flip-coil.[5] This device has a measured stability of better than 0.3% per 10 h, and was used to check and correct for drift in the current-regulator of the magnet. Corrections were always small and infrequently necessary, and for this reason the error introduced by fluctuations in the beam energy is considered negligible.

The electrons traveled inside a 3-in.-diam pipe about 30 ft into the end station where they left the vacuum system (to this point continuous with the accelerator vacuum system) through a 0.002-in. Duraluminum window. After passing through several inches of air, the collimated, momentum-analyzed electron beam penetrated a continuously moving secondary emission monitor ("wobbly SEM") previously described.[6] This instrument was relied upon to measure the incident-electron intensity used in calculating the photon intensity at the target. The stability of its calibration has been reported to be better than 1% over time periods of tens of hours of continuous usage; this finding was corroborated during each of the runs of this experiment by calibrating the SEM against the Faraday cup of the Electron Scattering Group.[7]

A clearing magnet was used to keep the electrons from hitting the target. After traversing a radiator, located behind the SEM, the electron beam was deflected downward through an angle of approximately 15° by the field of the clearing magnet. The electrons entered the scattering chamber through a 0.005-in. Dural window, passed below the targets and out the other side of the scattering chamber through another thin Dural window. For given electron energy the current in the clearing magnet was set by observing the position of the electron beam as it passed through the second window, either with a phosphorescent screen and television (continuously) or by the use of glass slides (intermittently). This was necessary because an improper setting of the current in the clearing magnet caused a noticeable increase in the background counting rate from the electron beam striking the lower

[3] K. L. Brown, Rev. Sci. Instr. **27**, 959 (1956).
[4] T. Janssens (private communication).
[5] F. A. Bumiller, Stanford High Energy Physics Laboratory Report No. HEPL-257, 1962 (unpublished).
[6] M. J. Bazin and J. Pine, Phys. Rev. **132**, 831 (1963).
[7] F. A. Bumiller and E. B. Dally, in *Proceedings of an International Conference for High-Energy Physics* (Interscience Publishers, Inc., New York, 1961), p. 305.

side of the target or the scattering chamber wall. The stability of the clearing magnet current-regulator obviated manual readjustment of the current except when the beam energy was changed.

B. Gamma Beam

Approximately 5 in. downstream of the wobbly SEM the electron beam passed through a 2-in.×2-in. aluminum radiator of selectable thickness, typically 0.022 radiation lengths. The radiators were mounted on a horizontally translating mechanism, the position of which was controlled and monitored to ±0.05 in. (The mean beam diameter at this point was typically $\frac{1}{8}$ in.) In addition to radiators, the translating mechanism held a ZnS-coated aluminum foil used in conjunction with a television monitor to position the radiators, and a blank used when calibrating the SEM and when taking elastic-electron-scattering data for normalization.

Contributions to the photon spectrum from various radiators in the path of the electron beam were calculated with a digital computer from the measured values of the incident-electron energy and intensity, and from the composition and thickness of each radiator. The program[8] accounted for finite radiator effects by folding the "thin-target" prediction of the bremsstrahlung spectrum over the radiator thickness. The calculation itself is probably valid to ±2%.

The photons entered the scattering chamber through a 0.005-in.-thick Dural window, passed through the target and out of the scattering chamber through the exit window, also constructed of 0.005-in.-thick Duraluminum. A remotely controlled CsBr crystal was positionable directly behind the exit window to check beam alignment and to set vertical target position. When in use, the crystal was viewed with a television camera, but while data were being taken the crystal was removed from the beam line to eliminate a possible source of background.

A quantameter[9] was used occasionally to check the calibration of the SEM during data collection. Information so gained increased our confidence in the reliability of the SEM by providing an independent check on the photon intensity. However, the background caused by the gamma beam striking the quantameter discouraged its full-time use.

C. Target

The target was similar to the "cigar-shaped" variety designed for use in electron-scattering experiments,[10] but of larger diameter to accommodate the photon beam. The target assembly consisted of two identical targets, each 1.71 in. in diameter and 8.25 in. long, with 0.001-in.-thick stainless steel walls. The targets were mounted one above the other; the upper target was filled with liquid hydrogen, and the lower was evacuated and used for background studies. The diameter of the photon beam as it passed through the targets was about 0.75 in., so beam alignment was checked frequently to minimize background caused by the beam striking the target walls.

For forward scattering ($\theta=0°$) the targets were oriented with the long axis of the target parallel to the beam line. This orientation was necessary to obtain a viable signal-to-noise ratio, the background being very high because of copious production of protons by the beam as it traversed the target walls and various vacuum windows, finally striking the back wall of the spectrometer vacuum chamber near the 45° port. The effective target length in this configuration is simply the physical target length.

The same orientation was employed for recoil-proton angles $\theta>20°$. In this orientation the effective target length t_e is predicted by geometrical considerations and first-order magnet theory to have the approximate form

$$t_e=(\text{counter width})/\sin\theta, \tag{1}$$

provided θ is large enough that particles emitted from the ends of the target will not be transmitted by the magnet. This form of the effective target length agrees within experimental uncertainties (<5%) with measurements of the magnet transmission made with a thin movable target at angles $40°\leq\theta\leq90°$, and momenta less than 650 MeV/c.[11] The angle at which the spectrometer will transmit particles emerging from the target ends is not known precisely, but is less than about 14° for conditions of this experiment. For small angles $0°<\theta\leq20°$, therefore, the long axis of the target was placed perpendicular to the beam line to provide a target of known thickness. In this case the correction due to finite beam size causes the effective thickness to have the form

$$t_e=D[1-(r/D)^2], \tag{2}$$

where D is the target diameter and r is the rms beam radius.

The density of the target hydrogen was not measured directly. However, pressure and temperature measurements of the hydrogen in a target similar to that used here indicated a temperature about 0.3°K higher than that predicted by the vapor-pressure curve for liquid hydrogen in equilibrium with its saturated vapor. We assume that a change of $\Delta\rho$ in the density ρ due to a change of pressure ΔP is approximately that for equilibrium liquid hydrogen, viz.,

$$\Delta\rho/\rho\simeq-\Delta P/330\ \text{psi}. \tag{3}$$

Pressure changes were observed as the hydrogen in the

[8] Dr. E. A. Allton kindly provided us with an improved version of the program described by R. A. Alvarez, Jr., Stanford High Energy Physics Laboratory Report No. HEPL-228, 1961 (unpublished).

[9] H. Fisher and C. Schaerf, Rev. Sci. Instr. **35**, 615 (1964).

[10] B. Chambers, R. Hofstadter, A. Marcum, and M. Yearian, Rev. Sci. Instr. **34**, 1019 (1963).

[11] E. F. Erickson, Ph.D. thesis, Stanford University, 1965 (unpublished).

target reservoir was dissipated, but these were never allowed to exceed 5 psi.

D. Spectrometer

To determine the momentum and angle of the final proton, the 72 in. radius, 180° double focusing magnetic spectrometer of the Electron Scattering Group was used. This device derived its momentum calibration from the known incident-electron energy. The current was set and the stability checked in a manner similar to that already described for the incident-electron deflection system. The solid angle and momentum acceptance of the detection system were limited by the counters and by baffles placed in the vacuum chamber of the magnet through ports at 90° and 135° (see Fig. 2).

The fractional momentum acceptance has been found to have the form

$$\Delta p/p = (\text{counter height})/297 \text{ in.} \quad (4)$$

varying less than about 3% for magnet field settings between 300 and 800 MeV/c.[12] The momentum dependence of the solid angle might be questioned because it is partly defined by the baffles which are in the magnetic field. However, the baffles limit the particle orbits to regions of the vacuum chamber where the shape of the field (n value) is rather insensitive to the field setting, particularly at settings less than 800 MeV/c.

The rotating coil occupied the 45° port except for the $\theta=0°$ measurements when it was removed to decrease background caused by its brass housing being struck by the gamma beam. The entrance window to the spectrometer vacuum chamber was 0.005-in. Dural, 24 in. from the target center. The spectrometer angle was reproducible to better than $\pm 0.1°$.[12]

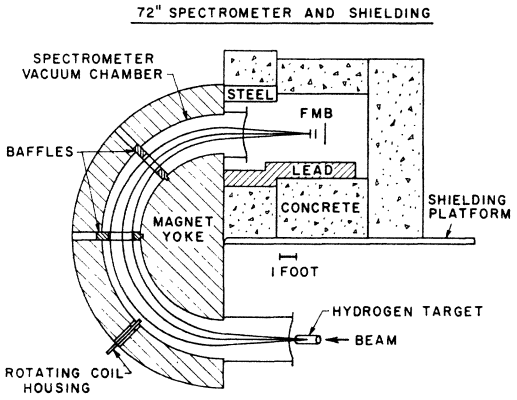

FIG. 2. Topography of the detection system. Particles leaving the target with the correct momentum are detected by the three plastic scintillation counters, F, M, and B. Baffles in the 90° and 135° ports serve to define the solid angle subtended by the detector: The rotating coil measures the magnetic field in the spectrometer vacuum chamber.

[12] F. A. Bumiller (private communication).

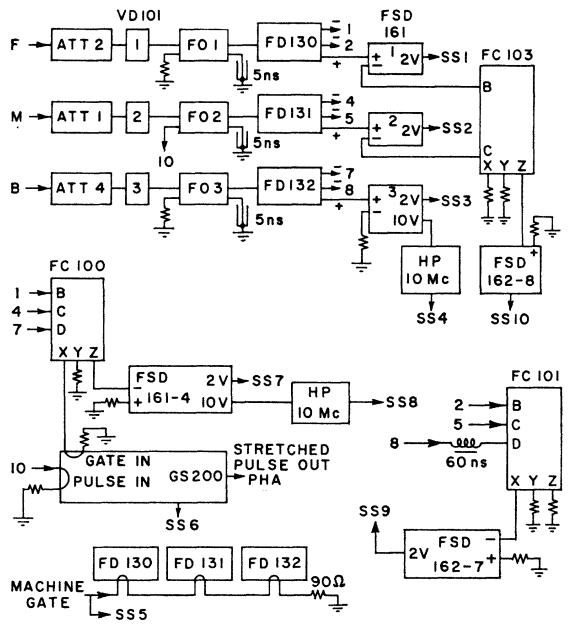

FIG. 3. Block diagram of electronics of detection system. Abbreviations are: ATT, attenuator; FO, fanout; FD, discriminator; FSD, scaler driver; FC, coincidence circuit; HP, 10-mc/sec scaler; SS, slow scaler; GS, gated stretcher; PHA, to pulse-height analyzer.

E. Counters and Electronics

The detection system consisted of three scintillation counters in coincidence. The first two scintillators were 2 in.×2 in., 0.25 in. and 0.375 in. thick, respectively, and were placed very close together. The third one was round, 4 in. in diameter, 0.25 in. thick and was separated 5 in. from the other two. (See Fig. 2.) They were labeled respectively: front, middle, and back. Front and middle were viewed by RCA 6810A photomultipliers through Lucite light pipes. The third, Back, was connected through a short piece of light pipe to the face of an RCA 7046 photomultiplier. The anode pulses from the photomultipliers were sent to the counting room via low-dispersion 50-Ω cables. In the counting room every pulse traversed a variable delay box, an attenuator, and a transistorized fanout (Fig. 3). Pulses from one output of each fanout were clipped and sent to regenerative tunnel-diode discriminators which were gated on only when the beam was on. The output pulses from the discriminators, typically 10 nsec full width at half-maximum (FWHM) were used to operate coincidence logic. While taking data we continuously measured:

1. single pulses emitted by the discriminators: SS1, SS2, SS3, SS4 (fast);
2. double coincidences between front and middle: SS10;
3. triple coincidences among all three discriminators: SS7, SS8 (fast);

4. triple coincidences with back delayed by 60 nsec: SS9;
5. triple-gated pulse-height spectrum from middle: PHA;
6. number of firings of the gated stretcher: SS6;
7. number of machine pulses: SS5.

The scalers used (denoted by SS in Fig. 3) had dead times long compared with the duration of a pulse from the accelerator. (The duration of a machine pulse is typically 800 nsec.) This method of operation increases the counting loss due to scaler dead time, but makes the correction independent of the duration of the accelerator pulses. This is important because the machine duty cycle is extremely dependent on tuning procedure and is poorly reproducible. Two of the channels were also monitored using faster scalers (10 Mc/sec). Counting losses were calculated for the slow and the faster scalers and found consistent.

The output pulse from the triple coincidence was also used to trigger a gated stretcher (GS200) which had an "on time" of about 40 nsec followed by a dead time of about 3 μsec. Pulses from one of the fanouts fed the input of this device. When a trigger pulse preceded the arrival of an input pulse by a few nsec, the gated stretcher produced an output pulse, the amplitude of which was proportional to the charge of the input pulse. These output pulses were sent to a multichannel pulse-height analyzer. The on-time and dead-time characteristics of the gated stretcher minimized effects of counting rate ("pileup") in the operation of the analyzer, and considerably decreased background in the recorded pulse-height spectra. When adjusting the discriminators, we fed pulses from each counter in turn to the gated stretcher. Pulse-height spectra from the middle counter were recorded as data. The identification of the protons amid the background of lighter and heavier particles of the same momentum was achieved by primary ionization in the scintillators. The three fast discriminators were set to preclude counting the minimum ionizing particles, which constituted the largest background.

III. ANALYSIS OF DATA

A. General Remarks

Data were taken on several weekend-length runs. Each point consisted of counting the number of protons from the hydrogen target for fixed spectrometer angle and field setting. The energy of the electron beam was set to exclude kinematically the possibility of counting protons from multipion production. Many of the points were repeated on different runs to check for possible systematic errors. For each point an empty-target background was also measured.

B. Processing of Data

Raw data from the multichannel analyzer and the scalers were punched on IBM cards and subsequently analyzed by a SUBALGOL[13] program in an IBM-7090 digital computer. From the recorded pulse-height spectrum the program formed a smoothed spectrum from which the position and half-width of the proton pulse-height distribution was determined. The number of counts in the original spectrum within ± 4 half-widths was then computed. Total counts between ± 3 and ± 5 half-widths were compared to the 4 half-width value to prove results were not sensitive to the integration interval. This method of analysis permitted final discrimination against light particles and the rejection of the heavier ones, while ensuring nearly 100% efficiency for counting protons.

The program used the information from the scalers to correct the number of proton counts for dead time and the delayed coincidence background, and computed the statistical error due to these corrections. The empty-target data were analyzed in a similar way, except that the pulse-height distribution was integrated over the same interval as the corresponding full-target spectrum. Finally the program normalized the number of proton counts to the number of incident electrons, made a "full minus empty" subtraction, and printed out the number of protons per microcoulomb with statistical errors for each datum point.

C. Normalization of Data

The expression for the number of events observed for a given number of electrons incident on the radiator is an integral of the photoproduction cross section over the bremsstrahlung spectrum, the target length, the solid angle, and the momentum of the recoil protons. The integral over the bremsstrahlung spectrum is calculated from kinematics, which determine the photon energy in terms of the momentum and angle of detected protons. The resulting expression may be well approximated, for conditions of this experiment, by the product of the cross section, the value for the bremsstrahlung intensity, appropriate kinematical factors, and an experimental aperture. This aperture, which we call N', is defined as the product of effective solid angle, effective target length, fractional momentum acceptance and detection efficiency. The value of N' must be known to determine absolute cross sections from the recorded counts per microcoulomb.

N' depends on the counter positions and sizes, the positions of the baffles in the magnet vacuum chamber, the orientation of the target, the magnetic field setting, the scattering angle, and the efficiency for recording true events. The value of N' was determined for each run by comparing measurements of elastic electron scattering from hydrogen with known values of the cross section for this process.[14] All of the data from a

[13] SUBALGOL, The Stanford University Algorithmic Language, Stanford University Computation Center, 1963 (unpublished).
[14] C. de Vries, R. Hofstadter, A. Johansson, and R. Herman, Phys. Rev. 134, B848 (1964).

run were normalized with the value of N' measured during that run, to cancel dependence of the photoproduction results on counter efficiency, and on counter and baffle geometry.

One of the momentum spectra of recoil protons from elastic electron scattering is shown in Fig. 4. The large tail on the low-momentum side of the elastic scattering peak is primarily due to photo- and electroproduction of neutral pions. The shape of this tail near photoproduction threshold was calculated by folding the bremsstrahlung spectrum with the experimental resolution. This prediction was normalized to the background-subtracted empirical spectrum, and subtracted to give the spectrum due to electron scattering alone. Radiative[15] and bremsstrahlung corrections were applied to the resulting peak at various values of the low-momentum cutoff, to check the validity of the π^0 subtraction. The largest deviation found in the area under the corrected spectrum of any of the seven elastic peaks analyzed was $\pm 3.7\%$ for a 10-MeV/c variation of the cutoff momentum.

The corrected area in an observed elastic-scattering peak, A_{ep} [with units (counts$\times$MeV/c)/μC], was used to calculate the experimental aperture from the formula

$$N' = (A_{ep}/P_{peak}')[Q\rho N_0 \sigma_R]^{-1}, \quad (5)$$

where P_{peak}' is the momentum corresponding to the field setting at the elastic peak, σ_R is the Rosenbluth cross section, N_0 is Avagadro's number, Q the number of electrons per microcoulomb, and ρ the density of liquid hydrogen. We express N' in units of steradian inches.

Comparison of the elastic-scattering results from the various runs provides a consistency check on several assumptions in the analysis, particularly the angular and momentum dependence of N'. Assuming the angular dependence of the effective target length (t_e) given in Sec. II C, we compare the value of N' obtained from the elastic peak taken with the target perpendicular to the beam with the N' values found from elastic-scattering data recorded with the target axis parallel to the beam by defining

$$N = N'(\text{counter width} \times t_e), \quad (6)$$

which should be independent of momentum, scattering angle, and target orientation. Table I summarizes the kinematics, calculated cross sections, and N values for elastic-scattering data. It is seen that values of N measured on the same run are in good agreement. The variation in N from run to run may be due to differences in counter geometry and/or counter efficiency. In any case the π^0 cross section is normalized to the elastic-scattering cross section, so N need only be constant through a run. The value of N calculated from first-order magnet optics is 0.47×10^{-4} steradian inches, assuming a counter efficiency of 100%.

The differential cross section for photoproduction in the center-of-mass system has the form

$$\frac{d\sigma}{d\Omega^*}(k,\theta^*) = n(P,\theta)\left[Q\rho N_0 \frac{\partial(k,\Omega^*)}{\partial(P,\Omega)}\frac{P}{k} f(k,E_0)N'\right]^{-1}, \quad (7)$$

where θ^* is the proton center-of-mass angle,[1] $n(P,\theta)$ is the number of photoproduction events per microcoulomb of electrons incident on the radiator resulting in protons recoiling with laboratory angle θ and momentum P, and $f(k,E_0)dk/k$ is the number of photons with energy between k and $k+dk$ produced per electron with

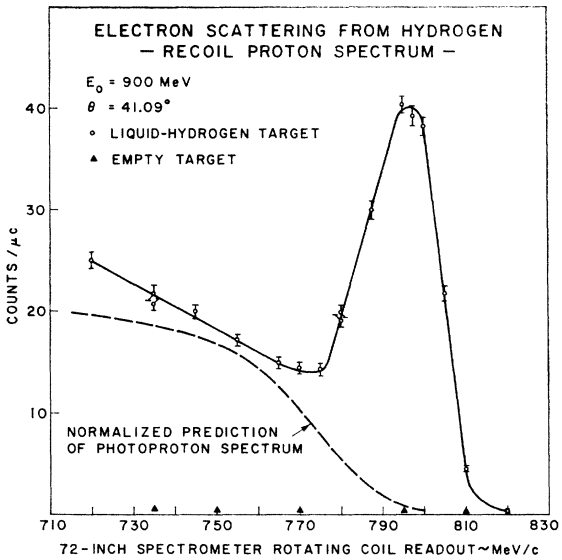

FIG. 4. Momentum spectrum of recoil protons detected at 41.09° with 900-MeV electrons incident on hydrogen target. The peak is due to elastic electron-proton scattering. The solid line is a visual fit to the experimental points and the dashed line the calculated recoil-proton spectrum for π^0 photoproduction. The difference between calculated and measured spectra in the continuum region near the elastic peak is due to radiative effects. Pion pair production threshold is near 720 MeV/c.

TABLE I. Summary of elastic-scattering data used to normalize photoproduction data to absolute cross sections. E_0 is the incident-electron energy, θ_p the laboratory angle of the scattered proton, P_{peak}' the momentum of the scattered proton, σ_R the Rosenbluth cross section, and N the experimental aperture. Values of σ_R were calculated from the "b'" fit to the proton form factors of Ref. 14. Errors on N, exclusive of errors on σ_R, are estimated to be less than 5%.

Run number	E_0 (MeV)	θ_p (deg)	P_{peak}' (MeV/c)	σ_R (10^{-32} cm^2/sr)	N (10^{-4} sr inches)
1	900	41.09	801	3.14	0.568
1	720	26.97	854	1.88	0.564
2	950	67.18	381	8.48	0.468
3	900	41.09	801	3.14	0.470
3	840	41.39	761	3.81	0.460
4	900	41.09	801	3.14	0.402
5	700	18.22	912	1.34	0.417

[15] N. Meister and D. R. Yennie, Phys. Rev. **130**, 1210 (1963).

TABLE II. Measured values of differential cross section in μb/sr with associated fractional errors. θ_p^* is the center-of-mass angle between incident photon and recoil proton and k the incident-photon laboratory energy in MeV.

θ_p^* \ k	660		680		700		720		740		760		780		800	
	$d\sigma/d\Omega^*$	$\Delta\sigma/\sigma$	$d\sigma/d\Omega^*$	$\Delta\sigma/\sigma$	$d\sigma/d\Omega^*$	$\Delta\sigma/\sigma$	$d\sigma/d\Omega^*$	$\Delta\sigma/\sigma$	$d\sigma/d\Omega^*$	$\Delta\sigma/\sigma$	$d\sigma/d\Omega^*$	$\Delta\sigma/\sigma$	$d\sigma/d\Omega^*$	$\Delta\sigma/\sigma$	$d\sigma/d\Omega^*$	$\Delta\sigma/\sigma$
0	0.922	0.064	1.081	0.064	1.155	0.063	1.25	0.040	1.29	0.040	1.361	0.050	1.078	0.030		
10	0.860	0.060	0.88	0.079	1.41	0.050	1.43	0.050	1.49	0.050	1.67	0.050	1.38	0.050		
20	1.12	0.080	1.217	0.071	1.364	0.060	1.69	0.057	1.95	0.049	1.65	0.050	1.67	0.045		
30	1.15	0.078	1.194	0.072	1.50	0.060			2.094	0.046	1.83	0.050	1.86	0.050		
40	1.441	0.069	1.50	0.059	1.88	0.053	2.265	0.043	2.174	0.046	2.43	0.080				
50	1.92	0.057	2.15	0.030	2.39	0.039	2.67	0.030	2.69	0.030	2.83	0.030	2.63	0.030	2.59	0.030
60	2.52	0.032	2.69	0.030	3.14	0.030	3.31	0.030	3.30	0.030	3.27	0.030	2.95	0.030	2.91	0.030
70			3.15	0.030	3.58	0.030	3.88	0.030	3.84	0.030	3.94	0.030	3.48	0.030	3.35	0.030
80			3.47	0.030	3.98	0.030	4.24	0.030	4.38	0.030	4.14	0.030	4.11	0.030	3.85	0.030
90			3.37	0.034	4.09	0.030	4.48	0.030	4.29	0.030	4.70	0.030	4.35	0.030	3.50	0.030
100	2.93	0.042	3.23	0.036	3.98	0.030	4.20	0.030	4.53	0.030	5.42	0.030	4.03	0.031	3.80	0.031
110	2.65	0.044	3.114	0.047	3.45	0.030	4.01	0.039			4.13	0.035	3.93	0.036	3.37	0.037
120	2.05	0.062	2.62	0.051	2.82	0.050	3.07	0.037	3.54	0.044	3.33	0.047	3.51	0.047	2.93	0.036
130	1.76	0.080			2.31	0.057	2.54	0.048	2.74	0.047	3.00	0.050	2.68	0.040	2.49	0.049
140									2.12	0.064	2.22	0.062	2.12	0.055	1.826	0.076

θ_p^* \ k	600		620		640		690		730		750		770		790	
0	0.517	0.130	0.731	0.088	0.802	0.078	0.980	0.064	1.254	0.050	1.389	0.043	1.312	0.045	0.809	0.054

energy E_0 incident on the radiator. For reference, the Jacobian is

$$\frac{\partial(k,\Omega^*)}{\partial(P,\Omega)}=\frac{P}{T_p+M}\,\frac{M+2k}{[(k-m_\pi^2/2M)^2-m_\pi^2]^{1/2}}\times\frac{P}{(P\cos\theta-T_p)}, \quad (8)$$

where m_π is the neutral pion mass, M is the proton mass, and $T_p=(P^2+M^2)^{1/2}-M$ is the kinetic energy of the proton. The kinematical relations

$$k=(MT_p+\tfrac{1}{2}m_\pi^2)/(P\cos\theta-T_p), \quad (9a)$$

$$-\cos\theta^*=\frac{k^2-\frac{1}{2}m_\pi^2(1+k/M)-T_p(M+2k)}{k[(k-m_\pi^2/2M)^2-m_\pi^2]^{1/2}} \quad (9b)$$

were used to deduce the magnetic field settings and spectrometer angles (P and θ) required to take the data points at evenly spaced values of k and θ^*. The estimated γ-ray energy resolution was a slowly varying function of energy. Typical values for $k=700$ MeV have been calculated to be 31, 18, and 7 MeV for $\theta^*=120°$, 90°, and 60°, respectively.

D. Errors

The absolute value of the density of the target hydrogen cancelled in the normalization procedure. Density fluctuations due to variations of the target pressure [cf. (3)–(7)] over the weekend runs caused an estimated 1.5% maximum uncertainty in the cross sections. The more exact integral expression from which (7) was derived as an approximation was used to estimate that resolution considerations result in negligible change in the analysis. Error in the momentum calibration of the spectrometer increased as the magnet went into saturation. We continuously monitored the current in the coils and the magnetic field in the spectrometer gap. Both quantities showed a nonlinear behavior at very high momenta. The use of calibration points to measure the amount of saturation gave confidence that the result of the interpolation and extrapolation from these points to the useful range of the momenta does not introduce an appreciable error into our data. The saturation of the magnet produced a change in the n value and therefore in the focusing properties. With lead slits placed in front of the magnet we were able to limit the particle trajectories to a very narrow beam around the central orbit. We measured the ratio of the yield of particles with very narrow slits and with slits completely open, and found that this ratio stayed constant as a function of magnet momentum. (The statistical accuracy of this measurement was better than 3%.) We therefore concluded that, while the focusing properties of the magnet might change as the magnet went into saturation, the phase space accepted remained constant.

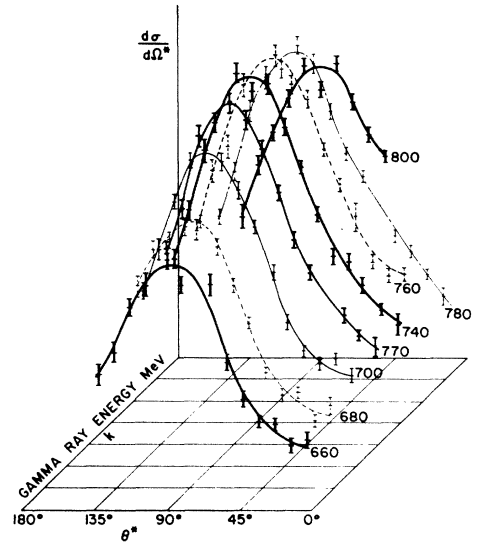

FIG. 5. Three-dimensional plot of measured angular distributions (see Table II and Figs. 6 and 7). The curves are visual fits to the data.

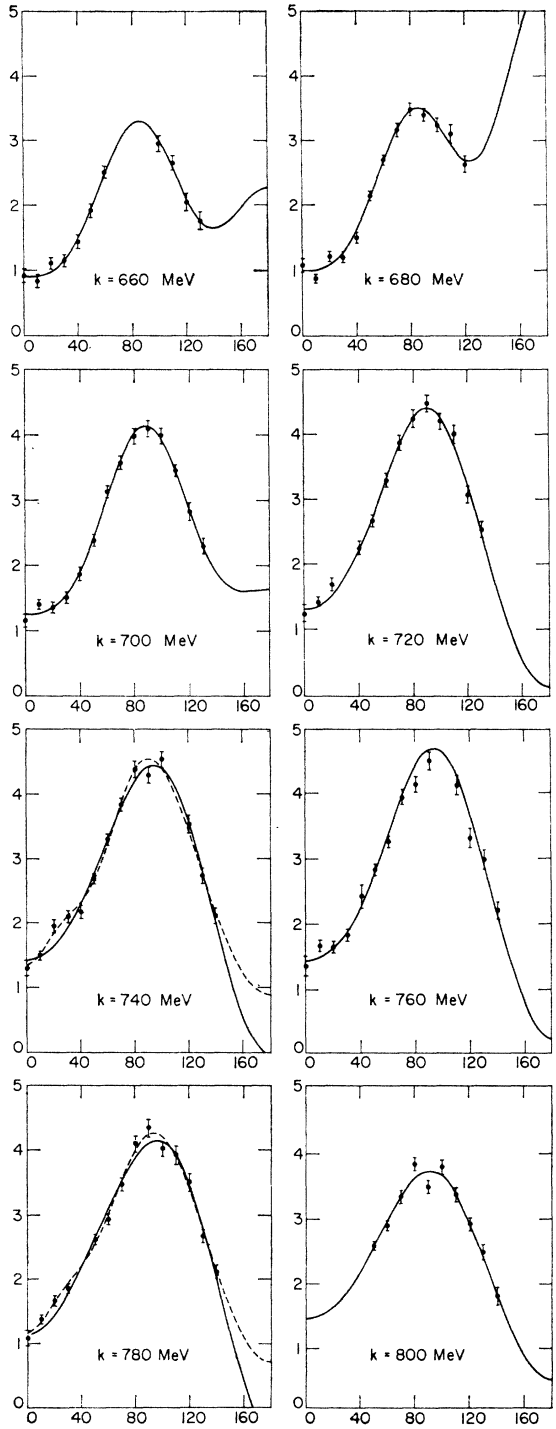

FIG. 6. Center-of-mass angular distributions for π^0 photoproduction. The ordinates are center-of-mass cross sections in microbarns per steradian, and the abscissas are the center-of-mass angle of the recoil proton in degrees. The solid curves are a polynomial fit to the data without crossed exchange contributions. The dashed curves include three crossed exchange poles as explained in the text. The masses of the exchange pole terms are $M_p=938$ MeV, $M_{33}=1230$ MeV, and $M_{\mathrm{VAR}}=1100$ MeV for $k=740$ MeV, and M_p, M_{33}, and $M_{\mathrm{VAR}}=1700$ MeV for $k=780$ MeV. In each case, four powers of $\cos\theta$ were used in the fits.

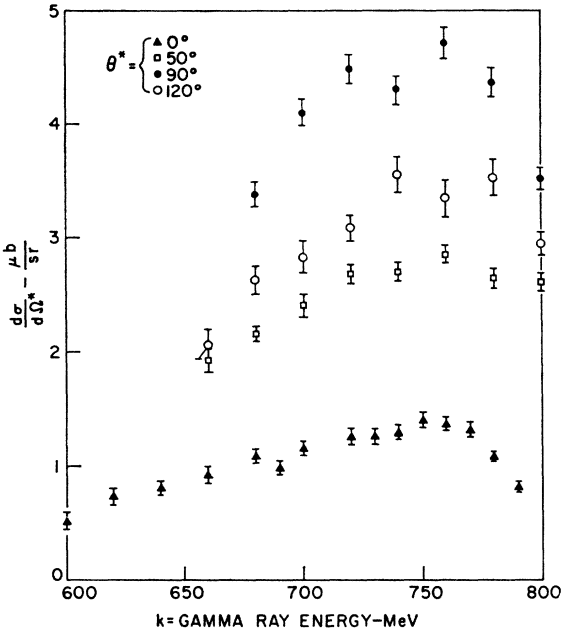

FIG. 7. Excitation curves at fixed center-of-mass angle.

Evidently the largest single source of error is the normalization. This means that the relative angular distributions taken in one single run are more accurate than the data taken on different runs. This error originates from the present limited knowledge of the electromagnetic form factors of the proton.

Elastic photon-proton scattering is also included in our data, but recent measurements[16] indicate that this contamination is not larger than 5%.

E. Experimental Results

The data taken on a weekend run were individually analyzed and, except at zero degrees, normalized to the appropriate elastic peak. To each point we assigned an error calculated solely from counting statistics unless this error was less than 3% in which case it was raised to 3% to allow for errors in normalization. All data from different runs corresponding to the same point were then combined according to their assigned weights. Again, any error below 3% was raised to this value. A different normalization procedure was necessary for the zero-degree data because of the high empty-target background. In this case they were normalized by considering an elastic peak for a different target and angle configuration, and by adjusting for the effective target thickness. Because of the possible uncertainty arising from this procedure, a 10% error was assigned to all zero-degree points before including them in the angular distributions. However, for the energy distribution at 0° the errors were calculated according to

[16] R. F. Stiening, E. Loh, and M. Deutsch, Phys. Rev. Letters **10**, 536 (1963).

TABLE III. Variation in $\eta(\chi^2/\text{d.f.})$ with n, degree of fitting polynomial.

k (MeV)	Degree of fitting polynomial 1	2	3	4	5	6
660	30.71	2.59	2.03	0.81	0.97	1.14
680	31.11	4.07	2.78	1.48	1.44	1.49
700	52.40	6.00	2.50	0.66	0.71	0.74
720	61.08	4.44	1.20	0.90	0.74	0.81
740	65.23	5.86	2.20	2.29	2.25	2.17
760	64.34	8.78	4.22	4.13	4.08	4.14
780	70.30	4.89	1.91	2.12	1.57	1.33
800	32.15	1.80	1.93	2.29	2.68	3.31

the method described for the other angles. These results are summarized in Table II and illustrated in Figs. 5–7.

IV. INTERPRETATION OF RESULTS

The shape of the total cross section as presented in Fig. 8 shows the expected resonant behavior in the 750-MeV region, and a comparison at 0° with the corresponding π^+ data[17] reveals that the discrepancy in the position of the resonance still exists. This establishes that the variation in position is not due to the direct photoelectric term (which cannot contribute at this angle). The angular-distribution curves would also indicate a slight enhancement at high-momentum transfer, a region not studied by previous experiments. A similar effect has already been observed in the low-momentum-transfer region in another experiment[18] and has been interpreted as the effect of peripheral exchanges as shown in Fig. 9(b). The enhancement seen in this experiment may be similarly explained in terms of the crossed nucleon and necleon isobar exchanges shown in Fig. 9(c). Both the peripheral and crossed diagrams of Fig. 9 correspond to poles in the scattering amplitude at positions outside the physical region in the $\cos\theta^*$ plane [whereas amplitudes for the direct scattering mechanisms in Fig. 9(a) have denominators

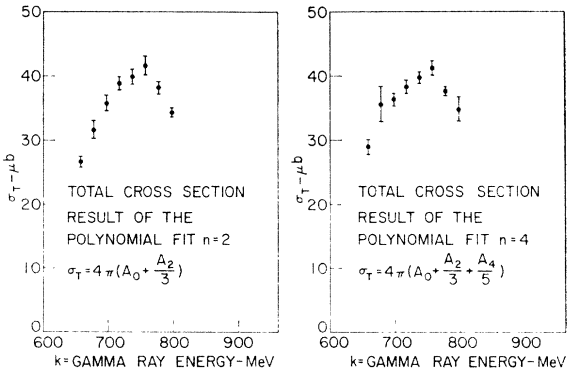

FIG. 8. Total cross-section curves as calculated from polynomial fit coefficients, for different degrees of fitting polynomial.

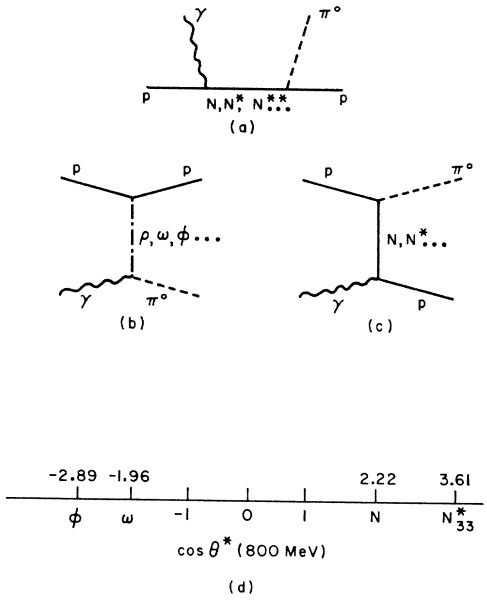

FIG. 9. Feynman diagrams for various pole contributions to this process. Direct, peripheral, and crossed terms are shown in (a), (b), and (c), respectively. The relative positions of the latter two pole terms in the $\cos\theta^*$ plane are shown at 800 MeV in (d).

which are not functions of $\cos\theta^*$]. Their positions, of course, depend on the energy, and are shown at 800 MeV in Fig. 9(d). We emphasize that, in our notation,[1] θ^* represents the center-of-mass angle between initial photon and final proton, so negative $\cos\theta^*$ corresponds to low-momentum transfer. As a pole contribution is expected to affect mostly the nearest part of the physical region, peripheral exchanges enhance the low-momentum-transfer region and crossed exchanges the high-momentum region.

In order to examine these effects further we have analyzed our data using the polynomial-fitting technique with which we assume the reader is familiar.[19] Each angular-distribution curve has been fitted with a polynomial in $\cos\theta^*$ up to the sixth degree. For each degree n of the fitting polynomial, we have obtained chi square divided by the number of degrees

TABLE IV. Coefficients of polynomial fit for $n=2$ with associated fractional errors.

k (MeV)	n	A_0	ΔA_0	A_1	ΔA_1	A_2	ΔA_2
660	2	2.88	0.10	0.20	0.15	−2.30	0.23
680	2	3.33	0.09	−0.11	0.24	−2.45	0.28
700	2	3.82	0.12	0.15	0.21	−2.94	0.30
720	2	4.12	0.11	0.20	0.17	−3.10	0.26
740	2	4.15	0.13	0.09	0.17	−2.93	0.27
760	2	4.32	0.16	0.00	0.21	−3.06	0.34
780	2	3.95	0.11	0.01	0.13	−2.76	0.22
800	2	3.72	0.07	0.07	0.09	−3.00	0.26

[17] L. Hand and C. Schaerf, Phys. Rev. Letters **6**, 229 (1961).
[18] R. M. Talman, C. R. Clinesmith, R. Gomez, and A. V. Tollestrup, Phys. Rev. Letters **9**, 177 (1962).
[19] A useful summary with references is given in the article by M. J. Moravcsik in *Dispersion Relations*, edited by G. R. Screaton (Oliver and Boyd, Edinburgh, 1961).

TABLE V. Coefficients of polynomial fit for $n=4$ with associated fractional errors.

k (MeV)	n	A_0	ΔA_0	A_1	ΔA_1	A_2	ΔA_2	A_3	ΔA_3	A_4	ΔA_4
660	4	3.27	0.11	0.76	0.28	−4.66	0.58	−1.46	0.78	2.99	0.90
680	4	3.47	0.08	0.64	0.34	−4.07	0.46	−2.06	1.44	3.58	1.20
700	4	4.14	0.06	0.34	0.22	−5.56	0.38	−0.62	0.63	3.013	0.69
720	4	4.40	0.07	0.01	0.24	−4.95	0.42	0.50	0.70	1.46	0.77
740	4	4.45	0.11	−0.55	0.35	−4.28	0.61	1.20	0.73	0.69	0.89
760	4	4.68	0.15	−0.65	0.42	−5.01	0.88	1.19	0.89	1.33	1.21
780	4	4.16	0.10	−0.66	0.28	−3.59	0.59	1.26	0.58	0.17	0.81
800	4	3.73	0.11	−0.14	0.31	−3.17	1.07	0.60	0.85	0.44	2.07

of freedom ($\eta=\chi^2$/d.f.), the coefficients of the polynomial ($A_0, \cdots, A_n$), and the statistical errors associated with these coefficients ($\Delta A_0, \cdots, \Delta_n$). The results of this analysis are shown in Tables III–VI. In Table III, we see a large drop in η from $n=1$ to $n=2$ and a minimum in η at all energies between $n=2$ and $n=5$. We find no satisfactory fit at 760 MeV and a significant variation from a good fit at several other energies. If one assumes that the observed resonance is mainly $d_{3/2}$ with background s and p effects, then the differential cross section may be represented as a polynomial of degree 2 of the form

$$d\sigma/d\Omega^*\equiv D_0(\cos\theta^*)=A_0+A_1\cos\theta^*+A_2\cos^2\theta^*. \quad (10)$$

The failure of our fit at several energies would indicate either a bad experiment at these energies or the effect of some mechanism such as the backward exchange mentioned earlier which is not well fitted by a polynomial. The reason for the latter fact is straightforward and has been discussed by many authors.[19] For completeness we repeat it here. If a single diagram of the form shown in Fig. 9(b) or 9(c) contributes to a process, then the differential cross section can be written in the form

$$D_0(\cos\theta^*)=[R(\cos\theta^*)]/(1-\beta\cos\theta^*)^2, \quad (11)$$

where $R(\cos\theta^*)$ is a polynomial in $\cos\theta^*$ and β determines the position of the particle exchange pole in the $\cos\theta^*$ plane [Fig. 9(d)]. Expanding the denominator in Eq. (11) as a power series in $\cos\theta^*$, we see that no polynomial of low enough degree will effectively fit the cross section. One must therefore make a fit to the function

$$D_1(\cos\theta^*)=(1-\beta\cos\theta^*)^2(d\sigma/d\Omega^*). \quad (12)$$

However, at least two more powers of $\cos\theta^*$ must now be used in fitting $D_1(\cos\theta^*)$ than were necessary in fitting $D_0(\cos\theta^*)$ with no crossed exchanges, and even more powers may be necessary if the exchanged particle has appreciable spin.

If more than one such pole diagram contributes, then one must fit a function of the form

$$D_m(\cos\theta^*)=(1-\beta_1\cos\theta^*)^2 \times(1-\beta_2\cos\theta^*)^2\cdots(1-\beta_m\cos\theta^*)^2(d\sigma/d\Omega^*). \quad (13)$$

More powers of $\cos\theta^*$ may now be necessary in the fit, although, if the β_i are sufficiently small, it may be possible to neglect higher powers of $\cos\theta^*$ in the expansion of the propagator product. There is, of course, a practical limit on the number of poles which can be added. From a statistical point of view, an increase in the degree of the fitting polynomial reduces the number of degrees of freedom in our fit with consequential increase in the errors associated with the results. Furthermore, there is a source of numerical uncertainty in the fit. By multiplying the experimental data by many terms of the form $(1-\beta_i\cos\theta^*)^2$ we produce a rapidly varying function of $\cos\theta^*$ to fit, and also rapid variations in the associated error terms. As a result, the error matrix (h_{hk} of Ref. 19) which is an essential part of the polynomial fitting procedure becomes ill-conditioned. A very high degree of numerical accuracy is therefore necessary in order to obtain a meaningful solution, and in the more difficult cases numerical routines with fifty-decimal-digit accuracy were necessary.[20]

In testing to see if such exchanges are contributing, there are two main approaches we can use. We can either assume that the unphysical region is well approximated by poles at the positions of the known resonance states and use these alone for fitting, or we can approximate the unphysical region by one or more poles and search for their best-fit positions. We have combined both methods and successively fitted the data with the crossed exchanges successively approximated by (i) one floating pole (at $\cos\theta^*=1/\beta_v$), (ii) a crossed

TABLE VI. Calculated values of total cross section in μb with associated fractional errors. Values of $B=3A_0+5A_2$ are also given.

k (MeV)	n	σ	$\Delta\sigma$	B	ΔB	n	σ	$\Delta\sigma$	B	ΔB
660	2	26.6	0.86	−2.86	0.96	4	29.0	1.28	−13.2	2.73
680	2	31.6	1.36	−2.26	1.36	4	35.5	2.81	−10.0	2.14
700	2	35.7	1.19	−3.21	1.33	4	36.3	0.98	−15.4	1.79
720	2	38.7	1.03	−3.16	1.12	4	38.3	0.99	−11.6	1.93
740	2	39.8	1.17	−2.22	1.09	4	39.7	0.83	− 8.0	2.87
760	2	41.5	1.42	−2.33	1.39	4	41.2	1.14	−10.0	4.09
780	2	38.1	0.93	−1.96	0.88	4	37.6	0.71	− 5.50	2.76
800	2	34.2	0.66	−3.82	1.12	4	34.7	1.90	− 4.64	5.09
1	2	3	4	5	6	7	8	9	10	11

[20] Cleve Moler, Jet Propulsion Laboratory Report No. 32-294, 1963 (unpublished).

TABLE VII. Results of polynomial fit for $n=4$ with one, two, and three crossed poles included. We have not included the results for the one-pole fit at $k=660$ and 680 MeV as there was no indication of a pronounced minimum at any definite value of the floating-pole mass.

k (MeV)	No poles η	One pole η	$M_{\text{best fit}}$	M_{low}	M_{high}	β_v
660	0.81					
680	1.48					
700	0.67	0.40	605	597	612	0.95
720	0.90	0.62	640	610	670	0.85
740	2.29	0.75	620	610	650	0.89
780	2.12	1.01	640	610	710	0.84
1	2	3	4	5	6	7

k (MeV)	No poles η	Two poles η	$M_{\text{best fit}}$	M_{low}	M_{high}	β_v	β_p
660	0.81	0.69	700	670	770	0.72	0.40
680	1.48	1.17	680	640	900	0.81	0.41
700	0.67	0.62	800	710	2000	0.57	0.42
720	0.90	0.47	850	750	970	0.51	0.43
740	2.29	0.84	770	710	860	0.61	0.43
780	2.12	1.01	1000	840	1300	0.40	0.44
1	2	8	9	10	11	12	13

k (MeV)	No poles η	Three poles η	$M_{\text{best fit}}$	M_{low}	M_{high}	β_v	β_{33}	$\beta_v+\beta_{33}$	Column 12
660	0.81	0.62	800	740	930	0.55	0.23	0.78	0.72
680	1.48	1.17	750	670	1400	0.63	0.23	0.86	0.81
700	0.67	0.63	1400	900	2000	0.19	0.24	0.43	0.57
720	0.90	0.47	1100	950	1650	0.31	0.25	0.56	0.51
740	2.29	1.07	1050	870	1600	0.32	0.26	0.64	0.61
780	2.12	1.01	1700	1200	2000	0.15	0.27	0.42	0.40
1	2	14	15	16	17	18	19	20	21

nucleon pole and a floating pole ($\cos\theta^*=1/\beta_p$, $1/\beta_v$, respectively), (iii) a crossed nucleon, crossed 33 isobar and floating pole ($\cos\theta^*=1/\beta_p$, $1/\beta_{33}$, $1/\beta_v$, respectively). In each case, we computed the position of best fit for the floating pole by searching for the value of $\beta(\beta_v)$ which gave minimum η. The results of this analysis for $n=4$ are given in Table VII and illustrated for the two-pole fit in Fig. 10. Table VII also gives the corresponding mass of the floating pole ($M_{\text{best fit}}$) and the range of masses (between M_{low} and M_{high}) for which η does not exceed its minimum value by 20%. The fits at 760 and 800 MeV showed no statistical improvement and have been omitted. In the cases shown in the table, it was found that four powers of $\cos\theta^*$ were sufficient for the fits, indicating that the products of the β_i in the expansion of the propagator product in (13) were small enough to be neglected. Table VII shows that: (i) A fit with one pole is a considerable improvement over the no-pole fit of the cross section. (ii) A fit with two poles is a slight improvement on the one-pole fit, but there is no improvement when a third pole is added. (iii) The best fit value for the mass of the floating pole increases as more poles are added.

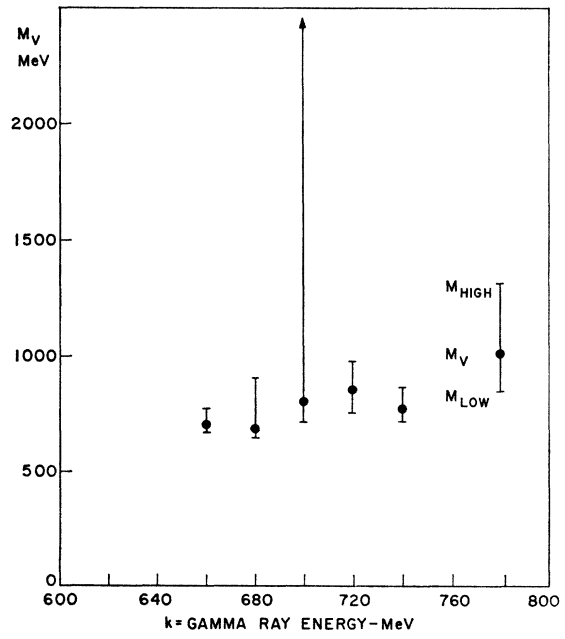

FIG. 10. Best-fit position of floating pole in two crossed-pole fit to data (see text).

We also attempted a fit with an extra pole in the peripheral region (corresponding to a vector-meson exchange) but there was no essential change in the fit, indicating that the enhancement could be explained solely in terms of crossed exchanges.

We emphasize that the method we have used does not yield any quantitative information on the physical processes involved, but is simply a convenient method

of parametrization. First, we are approximating the known crossed cut in the process by poles corresponding to the isobar states. This procedure, however, is expected to be reasonably accurate. Secondly, we see from Table VII that, in our experiment, the same results can be obtained if two poles are replaced by one of lower mass. In fact, in comparing the two-pole fit with the three-pole fit, we see (columns 20 and 21) that the β for the two-pole-fit floating pole is approximately the sum of the β_i for the two higher mass poles in the three-pole fit. This is suggested if one looks at the expression resulting when one tries to fit two actual poles by one. One is then approximating an expression of the form

$$\tilde{D}_1(\cos\theta^*)=\frac{(1-\beta\cos\theta^*)^2R(\cos\theta^*)}{(1-\beta_1\cos\theta^*)^2(1-\beta_2\cos\theta^*)^2} \tag{14}$$

by a polynomial, and searching for the value of β which gives minimum η. Writing $\tilde{D}_1$ in the form

$$\tilde{D}_1(\cos\theta^*)=\frac{(1-\beta\cos\theta^*)^2R(\cos\theta^*)}{(1-[\beta_1+\beta_2]\cos\theta^*+\beta_1\beta_2\cos^2\theta^*)^2}, \tag{15}$$

then we see that if

$$\beta_1+\beta_2<1 \tag{16}$$

and

$$\beta_1\beta_2\ll 1, \tag{17}$$

we might expect a best-fit position when

$$\beta\sim\beta_1+\beta_2, \tag{18}$$

although this is a very approximate rule, and may be influenced greatly by the structure of the numerator polynomial. Our result, however, that only four powers of $\cos\theta^*$ were necessary in all fits, would suggest that the condition (17) is sufficiently well satisfied in this case.

Our findings are a possible explanation for the fact that Talman *et al.*[18] at Caltech found a better fit to the low-momentum-transfer enhancement using a single peripheral exchange of a particle of mass of the order of the η than of the ω. It is now known that the η cannot contribute to this process (a neutral spinless particle cannot emit a photon), but, by our result, its mass could represent the exchange of two particles of higher mass, e.g., the ω and φ. To test this conclusion, we analyzed the data assuming that two poles, corresponding to the ω and φ, were contributing, and obtained a good fit. More significant, perhaps, was the fact that the estimated residue of the ω pole changed by an order of magnitude when two poles were used rather than one at the ω mass. We also found in our experiment that the estimate of the nucleon pole residue, for example, was off by several orders of magnitude from the calculated value (although the statistical errors were reasonably small) and changed drastically depending on the number of poles present.

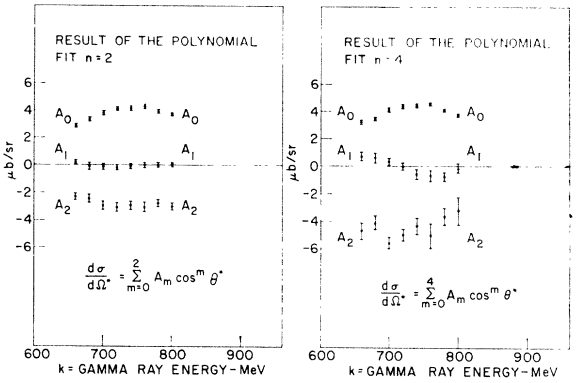

FIG. 11. Coefficients on polynomial fit for two values of degree of fitting polynomial.

This would seem to be a fair experimental indictment of the technique of pole extrapolation far from the physical region.

Our results also showed little dependence on the position of the fixed poles. Fits with these poles at other positions made little change, although the relation between the relative positions of the poles in the two- and three-pole fits still held. It does not seem possible, therefore, to obtain any information on the detailed structure of the exchanges involved by this technique. This could only be found by a direct calculation involving detailed knowledge of coupling constants and spin states occurring, which we have not attempted. We note in passing, however, that the data could be well fitted by three poles corresponding to the N, N^*, and N^{**} crossed states, but not if only the N pole was used.

If our interpretation of the observed high-momentum enhancement is correct, then this effect should also be observable at higher energies. There are, however, two mechanisms which could dampen the effect in such cases; first, although the singularities move nearer the physical region with increasing energy, their residues seem to decrease, and so their effect could in fact de-

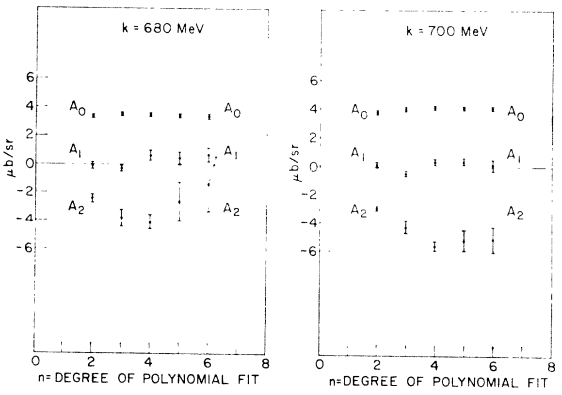

FIG. 12. Variation of polynomial coefficients with degree of fitting polynomial at 680 and 700 MeV.

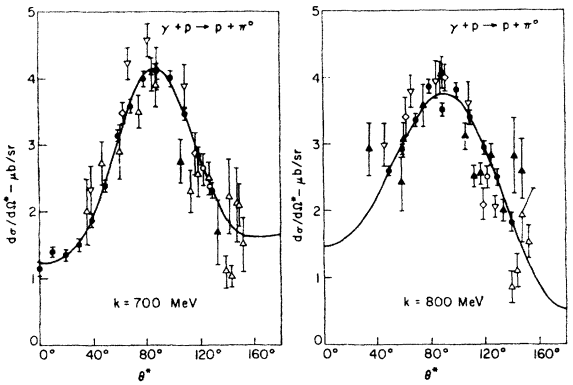

FIG. 13. The results of this experiment (indicated by ●) are compared with the following data: △ Berkelman and Waggoner; ▲ Vette; ▽ Worlock; ◇ Stein; ○ Diebold; × Frascati; which have been taken from Ref. 22.

crease rather than increase. Second, any "Reggeization" of these crossed exchanges would diminish the effect further. It would be useful, therefore, to examine the process in the 1- or 2-BeV region before drawing any further conclusions.

Our results, of course, indicate that this crossed-pole effect, if present, is reasonably small, and therefore the coefficients as we have presented them in Tables IV and V give reliable information on the contributions of the direct channels as shown in Fig. 9(a). The coefficients A_0, A_1, and A_2 are also given in Fig. 11. A_0 indicates a clear resonant behavior centered at 750 MeV. A_1 is very small and often consistent with zero. There is some evidence that it changes sign at the resonant energy. A_2 is large and negative and its absolute value decreases after the resonance.

In order to consider the coefficients we determined from the experiment, we require not only that the associated errors are smaller than the absolute value of the coefficients, but also that the value of the coefficient is not a rapidly varying function of the degree of the fitting polynomial. To illustrate the latter condition, we have plotted the coefficients as a function of the degree of the fitting polynomial for two particular energies in Fig. 12. We find that this condition is well satisfied by A_0, partially satisfied by A_1 and A_2, and never satisfied by A_3 and A_4. Consequently, we do not consider that the values we have found for A_3 and A_4 are physically meaningful, but including them does improve the fits.

If the observed resonance is well described as a $d_{3/2}$ effect, then it is expected that the differential cross section will have the form

$$d\sigma/d\Omega^* \propto (5-3\cos^2\theta^*). \tag{19}$$

We notice that the sign and magnitude of our coefficients is consistent with such an effect plus background terms. In columns 5, 6, 10, and 11 of Table VI we have tabulated the quantity $B=3A_0+5A_2$ and its associated error. Its value gives an indication of the deviation of the differential cross section from pure $d_{3/2}$. In the absence of any suitable theory to describe the seemingly complicated structure of the s and p waves in this region found in recent pion-nucleon analyses,[21] we have not attempted to analyze the results further.

The total cross section can be readily found from the coefficients and has the form

$$\sigma=4\pi(A_0+\tfrac{1}{3}A_2+\tfrac{1}{5}A_4). \tag{20}$$

We have plotted this for fits with polynomials of degree 2 and 4 in Fig. 8. The associated errors have been computed, taking into account the fact that the errors in the coefficients are not statistically independent. As noted earlier, the shape of the total cross section indicates a very pronounced resonance centered around 750 MeV.

To compare our results with previous experiments,[22] we have examined the available angular distributions and find that the present results are consistent with previous data. A comparison at 700 and 800 MeV is shown in Fig. 13.

V. CONCLUSION

The results of this experiment confirm that the angular distributions for this process in the region of the second pion-nucleon resonance are not in contradiction with a description in terms of a strong $d_{3/2}$ resonance state and background s- and p-wave effects. At the same time, the distributions cannot be effectively fitted unless it is assumed that some other mechanism such as crossed particle exchange is responsible for the observed high-momentum-transfer enhancement. The validity of this interpretation can be tested by further experiments at higher energies.

ACKNOWLEDGMENTS

It is a pleasure to thank Professor W. C. Barber and Professor R. Hofstadter for continued support and encouragement; and, in addition, Professor F. Bumiller, Professor S. D. Drell, Professor H. W. Kendall, Professor R. F. Mozley, Professor B. Richter, Professor L. I. Schiff, and Dr. P. A. M. Gram for many helpful discussions. The assistance of L. Boyer, J. Grant, and M. Ryneveld in setting up the experiment and of the machine crew, headed by Dr. P. B. Wilson and R. G. Gilbert, for continuous and reliable machine operation is also gratefully acknowledged. We also thank C. Moler (Stanford Computation Center) and L. Dall'Olio (Centro di Calcolo del C. N. E. N., Bologna) for considerable advice on the computing.

[21] For example, L. D. Roper, Phys. Rev. Letters **12**, 340 (1964).
[22] See Ph. Salin, Nuovo Cimento **28**, 1294 (1963).